Journal of Biomedical Optics

BiomedicalOptics.SPIEDigitalLibrary.org

Optical spectroscopic characterization of human meniscus biomechanical properties

Juho Ala-Myllymäki
Elvis K. Danso
Juuso T. J. Honkanen
Rami K. Korhonen
Juha Töyräs
Isaac O. Afara

SPIE.

Juho Ala-Myllymäki, Elvis K. Danso, Juuso T. J. Honkanen, Rami K. Korhonen, Juha Töyräs, Isaac O. Afara, "Optical spectroscopic characterization of human meniscus biomechanical properties," *J. Biomed. Opt.* **22**(12), 125008 (2017), doi: 10.1117/1.JBO.22.12.125008.

Optical spectroscopic characterization of human meniscus biomechanical properties

Juho Ala-Myllymäki,[a,b,*] Elvis K. Danso,[c] Juuso T. J. Honkanen,[d] Rami K. Korhonen,[a,b] Juha Töyräs,[a,b] and Isaac O. Afara[a,b]
[a]University of Eastern Finland, Department of Applied Physics, Kuopio, Finland
[b]Kuopio University Hospital, Diagnostic Imaging Center, Kuopio, Finland
[c]Colorado State University, Department of Mechanical Engineering, Fort Collins, Colorado, United States
[d]Kuopio University Hospital, Cancer Center, Kuopio, Finland

Abstract. This study investigates the capacity of optical spectroscopy in the visible (VIS) and near-infrared (NIR) spectral ranges for estimating the biomechanical properties of human meniscus. Seventy-two samples obtained from the anterior, central, and posterior locations of the medial and lateral menisci of 12 human cadaver joints were used. The samples were subjected to mechanical indentation, then traditional biomechanical parameters (equilibrium and dynamic moduli) were calculated. In addition, strain-dependent fibril network modulus and permeability strain-dependency coefficient were determined via finite-element modeling. Subsequently, absorption spectra were acquired from each location in the VIS (400 to 750 nm) and NIR (750 to 1100 nm) spectral ranges. Partial least squares regression, combined with spectral preprocessing and transformation, was then used to investigate the relationship between the biomechanical properties and spectral response. The NIR spectral region was observed to be optimal for model development ($83.0\% \leq R^2 \leq 90.8\%$). The percentage error of the models are: E_{eq} (7.1%), E_{dyn} (9.6%), E_{ε} (8.4%), and M_k (8.9%). Thus, we conclude that optical spectroscopy in the NIR range is a potential method for rapid and nondestructive evaluation of human meniscus functional integrity and health in real time during arthroscopic surgery.
[DOI: 10.1117/1.JBO.22.12.125008]

Keywords: meniscus; mechanical properties; visible spectroscopy; near-infrared spectroscopy; partial least squares regression.

Paper 170528R received Aug. 8, 2017; accepted for publication Nov. 27, 2017; published online Dec. 23, 2017.

1 Introduction

The menisci function as secondary stabilizers[1,2] and facilitate load distribution in the knee joint.[3] They contribute to joint lubrication,[4] nutrition of articular cartilage,[4] and proprioception.[5] The meniscus is composed of extracellular matrix (ECM) and fibrochondrocytes. The ECM consists mainly of interstitial fluid, various types of collagen, and in smaller proportions, proteoglycan (PG) macromolecules, and elastin.[6] The proportions of the different collagen types vary between anatomical locations, but type I collagen is predominant.[7] Meniscus is organized structurally in a layered architecture, with varying collagen types and structures in the different layers.[8] The concentrations of water, collagen, and PG in meniscus are site- and depth-dependent. Meniscus is partially vascularized, and based on its vascularity, it can be divided into three different regions: the fully vascularized peripheral region (red–red zone), the partially vascularized mid region (red–white zone), and the inner avascular region (white–white zone).[9] This difference in blood supply to the different zones of meniscus is directly related to its repair and regeneration capacity after trauma or injury. It has been shown that as the composition, structure, and morphology of meniscus change, its functional properties also change.[10]

The functional properties of meniscus deteriorate due to injury and/or aging.[11,12] Meniscal injuries are common in sports where there are risks of exposure to high peak stresses.[13] During degeneration, meniscus water content increases, while its collagen and PG contents decrease,[11] resulting in alteration of its biomechanical properties.[14,15] Since the menisci mainly perform biomechanical function, estimation of their biomechanical properties is essential when assessing their integrity. In addition, characterization of meniscus biomechanical integrity is important for evaluation of joint function and assessment of the risks of joint degeneration.

Currently, assessment of meniscal injuries are based on clinical examination, followed by radiography and/or magnetic resonance imaging, with repair performed during arthroscopic surgery. However, evaluation of joint tissue injuries and degeneration during arthroscopy is limited by its poor intra- and inter-observer reliability, and is often restricted to assessment of the superficial tissue.[16–18] Thus, there is a need for methods that can eliminate subjectivity while enabling deep tissue probing and quantitative evaluation in real time during surgery.

Several promising optical methods are being investigated for evaluating musculoskeletal tissues including near-infrared (NIR) spectroscopy,[19–24] midinfrared spectroscopy (mid-IR),[25] and optical coherence tomography.[26] NIR spectroscopy is a fast, nondestructive method that can be applied in real time for diagnosis. It is based on vibrations of polar anharmonic bonds (e.g., C—H, N—H, and O—H) in organic materials,[27] with wide absorption peaks resulting from overtone and combination vibrations.[27] This method has shown promising results in the characterization of articular cartilage biomechanical properties,[19,22] histological score,[28,29] and biochemical composition.[30,31] The solid matrix

*Address all correspondence to: Juho Ala-Myllymäki, E-mail: juhoala@uef.fi

1083-3668/2017/$25.00 © 2017 SPIE

of articular cartilage consists mainly of type II collagen, whereas that of meniscus consists primarily of collagen type I. Although the macromolecular chains of both collagen types are different, their structures have profound similarities.[32]

In the present study, the potential of light in the visible (VIS) region for assessing human meniscus biomechanical properties was also investigated.[33] The motivation for this is based on existing literature where the potential of light in the VIS spectral region for characterizing articular cartilage was demonstrated.[29,34] Recently, we demonstrated the capacity of NIR spectroscopy to predict the composition of the human meniscus.[33] Since the meniscus has similar composition as articular cartilage,[11,12] we hypothesize that there is a relationship between the biomechanical properties of human meniscus and its NIR optical response. The motivation behind this hypothesis is a combination of the structure (composition)–function relationship of meniscus and the correlation between the spectral response and the composition of meniscus, established in our recent study.[33] We test our hypothesis by investigating the relationship between meniscus spectral response and its biomechanical properties, evaluated by indentation testing and computational modeling using multivariate statistical technique based on partial least squares (PLS) regression.

2 Materials and Methods

2.1 *Sample Preparation*

Medial and lateral menisci were obtained from human cadavers ($N = 12$, 11 males, 1 female; 24 to 76 years old, mean age = 51.9 years), with no history of joint disease. The thickness of the samples at the measurement location varied from 2.4 to 7.8 mm with mean and median thicknesses of 4.0 and 3.9 mm, respectively. The human cadaver knees were obtained from Central Finland Central Hospital, Jyväskylä, Finland, under ethical approval by the National Authority for Medicolegal Affairs, Helsinki, Finland (permission 1781/32/200/01). After extraction from the joint, each meniscus sample was wrapped in a saline-soaked gauze. To prevent freeze drying, the gauze wrapped samples were sealed in airtight ziplock bags prior to storage at −20°C. Since the samples were frozen after extraction from the cadaver knee joints due to logistics and time constraints, freezing may have induced slight changes in their biomechanical properties.[35–37] However, since the storage condition was consistent for all the samples, any storage-induced changes in the tissue properties are expected to be systematic. When required, the samples were thawed by immersing the ziplocked bags in a water bath at room temperature; the samples were then immersed in phosphate buffered saline (PBS) supplemented with inhibitors of proteolytic enzymes: ethylenediaminetetraacetic acid dehydrate (EDTA; VWR International, Fontenay-sous-Bois, France) and benzamidine hydrochloride hydrate (Sigma-Aldrich Inc., St. Louis, Missouri).

2.2 *Biomechanical Testing*

The intact nonexcised meniscus sample was glued on a sample holder, and mechanical nondestructive indentation tests were then performed at premarked sites on the meniscus (anterior, central, and posterior) while fully immersed in PBS containing protease inhibitors.[15] Indentation tests were kept nondestructive (20% of tissue thickness) to preserve the biomechanical integrity of the tissue and its surface continuity during testing.

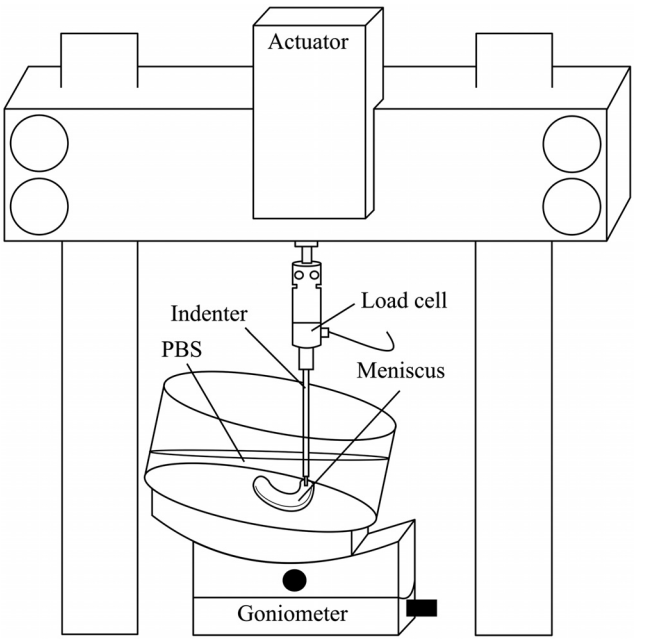

Fig. 1 Illustration of the biomechanical measurement setup.

Preservation of the biomechanical integrity was confirmed based on qualitative histological analysis from thin slices taken at the indentation sites. Mechanical testing was conducted using a custom-made material testing system[38] equipped with a high-precision load cell (model 31/AL311AR, Honeywell, Columbus, Ohio; resolution: 0.005 N) and an actuator (PM1A1798, Newport Corporation, Irvine, California; resolution: 0.1 μm). The transparent PBS-filled measuring chamber was tilted such that the indenter was perpendicular to the meniscus surface (Fig. 1). Indentation was performed using a cylindrical stainless steel indenter with a polished impermeable plane-ended tip ($d = 1.19$ mm). Contact between the indenter tip and meniscus surface was verified visually. In addition, a pre-stress of 6 kPa was applied. Dynamic pre-conditioning (sinusoidal loading, 2% strain, four cycles) of the sample was performed after the relaxation. With a ramp rate of 100% s^{-1} and a <10 Pa min^{-1} relaxation criterion, four compressive steps (5% of remaining meniscus thickness per step) were applied. The applied strain rate (5% of meniscus thickness per step, with 100% s^{-1} strain rate) is within the physiological levels of *in vivo* loading.[39,40] After the stress-relaxation test, the dynamic test was conducted using sinusoidal cycle with an amplitude of 2% of the remaining meniscus thickness at a frequency of 1 Hz.[15] After biomechanical testing, samples were allowed to fully recover and equilibrate in 0.15-M PBS.

2.3 *Analysis of Biomechanical Tests*

Equilibrium modulus E_{eq} was calculated from the experimental stress-relaxation data by assuming the tissue as elastic and isotropic,[38] taking the tissue thickness and indenter diameter into consideration as follows:[41]

$$E_{eq} = \frac{(1-\nu^2)\pi a}{2\kappa h}\frac{\sigma}{\varepsilon}, \tag{1}$$

where ν is the Poisson's ratio, a is the radius of the indenter, κ is the theoretical scaling factor, h is the tissue thickness, and $\frac{\sigma}{\varepsilon}$ is the slope of the last three steps of the stress–strain curve, fitted to

data points just before the next indentation step when the meniscus is in a relaxed state. Poisson's ratio of $\nu = 0.3$ used in the calculation of equilibrium modulus was based on the average value calculated indirectly from three bovine menisci.[15,38] For the calculation of the dynamic modulus (E_{dyn}, 1 Hz), a Poisson's ratio of $\nu = 0.5$ (incompressible material, i.e., no volume loss) was used based on the assumption of insufficient time for the fluid to flow out from the structure in fast loading.[42]

For further biomechanical analyses, the meniscus was modeled as a fibril-reinforced poroelastic (FRPE) material using the finite-element (FE) method. Biomechanical modeling was performed according to the protocol described in Danso et al.[15] FRPE models are able to separately determine the mechanical effects of the main constituents of soft tissues.[15,43–45] An axisymmetric model with porous elements (CAX8RP) was used to speed up the modeling analyses. To verify if the axisymmetric assumption is valid, a verification test with a 3-D model was conducted based on cone beam computed tomography image stack of a representative sample.[15,46] The axisymmetric model was created for each measurement site (anterior, central, and posterior, $n = 72$). The indenter was modeled as rigid and the bottom of the meniscus was set impermeable and fixed in all directions. Also, all free surfaces with no contact were assumed to be fully permeable (zero pore pressure), and the axis of symmetry and the contact between the indenter and meniscus (nonporous indenter) were assumed to be impermeable. The material parameters comprised the FRPE properties, developed earlier for cartilage.[38,43,47] We concentrated on obtaining the material properties of the samples, and as the model captured well all four steps with different strains, utilizing different loading protocols should not affect the modeling results.

The FRPE material consists of a fibrillar matrix (collagen network) embedded in a porous, nonfibrillar matrix (PGs) filled with interstitial fluid. The (solid) collagen network was modeled using nonlinear fibrils that resisted only tension determined as the initial and strain-dependent fibril network modulus (E_ε). The nonfibrillar matrix was modeled as a nonlinear neo-Hookean porohyperelastic material. Fluid flow through the tissue matrix was modeled with void ratio-dependent permeability, where (M_k) is the permeability strain-dependency coefficient.[48]

All FE analyses were conducted using Abaqus V6.12-3 (Dassault Systèmes Simulia Corp., Providence, Rhode Island), where the FRPE material was implemented using a user-defined material script. Using MATLAB (ver. R2010a, MathWorks, Natick, Massachusetts), the reaction force curve from each sample- and site-specific axisymmetric FE model was fitted to the corresponding experimental curve by minimizing the mean square error between the curves with a built-in minimization algorithm (fminsearch). The strain-dependent parameters were obtained from this optimization.

2.4 *Optical Spectroscopy of Meniscus Samples*

After biomechanical testing, samples were extracted from the different anatomical locations of the intact menisci (Fig. 2). From these samples, optical spectroscopy was then performed using an Avantes spectrometer (spectral range 200 to 1150 nm, AvaSpec-ULS2048XL, Avantes BV, Apeldoorn, the Netherlands) fitted with a diffuse reflectance fiber optic probe (optic probe diameter, $d_{probe} = 3.0$ mm and optic fiber core diameter, $d_{fiber} = 0.5$ mm) for acquiring the spectral response of the specimen. A custom-made light source ($P = 40$ W) was used to

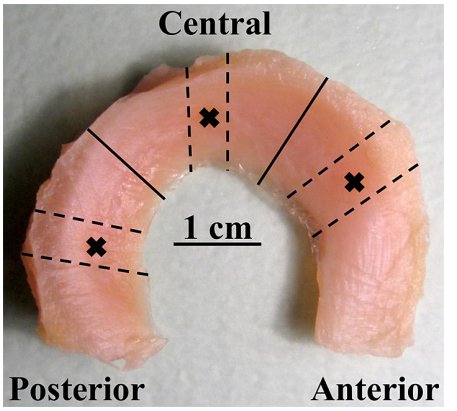

Fig. 2 Meniscus sample preparation showing the anatomical locations selected for measurements. Optical spectroscopy was performed for samples extracted between the dashed lines.

irradiate the sample (optical power ~18 mW at the sample surface), with wavelength range covering the VIS and short NIR spectrum. The experimental setup consisted of an optic fiber probe positioned opposite to the light source and at 45-deg angle relative to the specimen's surface (Fig. 3). The angle of the probe and light source were optimized based on preliminary studies. Optical measurements were acquired from a slightly larger tissue volume due to the nature of the experimental setup, in which the fiber optic probe was positioned about 2 cm above the sample. Nevertheless, this does not affect the overall outcome of this study as the biomechanical measurement location was within the central area, where the optical measurement was performed. More so, the surrounding tissue influences the biomechanical properties of the sample at the site of measurement.[49]

A single spectrum, obtained as the average of eight coadded scans, was collected from the central area of each sample. The spectrometer is equipped with a broadband detector that allows simultaneous spectral measurement at discrete wavelengths within the detector band. The spectrometer integration time (i.e., scan time) was set to 100 ms, resulting in a total spectral acquisition time of about 1 s per sample (~800 ms to acquire eight spectra that are then averaged to obtain the final spectrum). This very short spectral acquisition time reduces/eliminates the risk of the sample drying during measurement. Furthermore, the samples were kept moist with PBS during the setup and excessive PBS was wiped off before spectral acquisition. Spectroscopic measurements were performed in a relatively

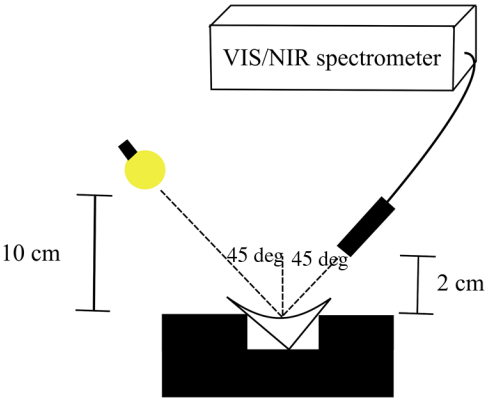

Fig. 3 Illustration of the spectroscopic measurement setup. The meniscus sample was fixed using a sample holder.

dark room and no preparation of tissue surface was required. Prior to spectroscopic measurements of the meniscus specimens, reference spectrum was measured from a polytetrafluoroethylene-based material, which has 94% reflectance across the wavelength range.

Spectral data were acquired at a resolution of 0.6 nm between 200 and 1150 nm. The results were formatted as a 1234-dimensional vector, where each vector element represents spectral intensity (absorption value) at a specific wavelength.

2.5 *Spectral Preprocessing, Multivariate, and Statistical Analyses*

Optical spectral data are often highly multicollinear and thus a technique, which is capable of de-correlation and feature extraction such as PLS, is required to relate this multidimensional data to reference measurements. The spectral data (predictor variables) for all specimens were correlated with their experimentally measured biomechanical properties (response variables) using PLS regression technique.[27] This statistical method is defined as

$$y_i = b_0 + \sum_{k=1}^{K} x_{ik}\hat{b}_k, \tag{2}$$

where x_i is measured spectral data, y_i is the i'th sample's predicted data, b_0 is the regression constant, $\hat{b}_k$ = regression coefficient, and $k = 1, 2, \ldots, K$ (number of predictor data points, $K = 1234$ when the full spectral data are used as predictor variable). Optimal use of this PLS multivariate technique requires correct selection of the number of components, which represents the number of latent variables to include in the development of the predictive model.[27] Only components that represent significant variance in the data are considered in the model development, and the efficiency of the developed model is tested using validation techniques. Too many or too few components would lead to over-fitting or under-fitting, respectively.

To test the effect of different preprocessing methods on the accuracy and performance of developed models, spectral analysis was performed using the raw spectrum, spectral derivative (Savitzky–Golay second derivative), scatter corrective methods (standard normal variate and multiplicative scatter correction). A third-order Savitzky–Golay smoothing with window size of 45 data points was used during second derivative pre-processing. Multivariate analyses were then performed for the NIR range (750 to 1100 nm).

K-fold cross validation (where $k = 6$) was used to estimate the error of each model. In this method, each sample is used in both training and validation of the model. The samples are divided into six equal groups (folds), where one fold contains the samples from two patients. One fold is left out (for validation) to be predicted with the model that is developed with the remaining folds. The process is repeated until all the folds have been used for validation. Root mean square error (RMSE) was calculated from each cross-validation round and finally averaged as root mean square error of cross-validation (RMSECV). The optimal model selection was determined by minimizing the number of components, RMSECV, and RMSEP while maximizing the coefficient of determination (R^2). Prediction error and coefficient of determination were defined from the final model where all the samples were used for the model development. RMSE was evaluated as follows:

$$\mathrm{RMSE} = \sqrt{\frac{1}{n}\sum_{i=1}^{n}(y_i - \overline{y})^2}, \tag{3}$$

where n is the number of samples, y_i is the i'th predicted response during cross validation, and $\overline{y}$ is the mean of measured responses. Spectral preprocessing and PLS analyses were performed using custom-written script in MATLAB (ver. R2014a, MathWorks, Natick, Massachusetts).

To test the effect of repeated measures, as multiple samples were obtained from each subject, differences in reference biomechanical properties between meniscus samples obtained from each subject were evaluated using generalized linear mixed model in SPSS (ver. 21.0, IBM Corp., Armonk, New York). Prior to the analysis, the samples were divided into six groups, representing samples from anterior, central, and posterior measurement sites in the lateral and medial menisci. These were considered as fixed variables, whereas the subjects were considered as random variables.

2.6 *Histological Evaluation*

For histological evaluation, 3-μm-thick sections were extracted from locations adjacent to the samples used for biomechanical and optical measurements, and stained with Safranin-O according to the protocol described in Honkanen et al.[46] Safranin-O is a cationic dye that binds stoichiometrically to the negatively charged glycosaminoglycans, which is indicative of the PG content of the tissue. PG content is an important factor affecting the biomechanical properties of meniscus.[12]

3 Results

The differences between the specimens' spectra in the NIR region were consistent with variations in meniscus biomechanical properties (Figs. 3 and 4). The water content in the different anatomical locations, which influences meniscus biomechanics, depends upon whether the medial or lateral meniscus was being examined, with higher water content observed in the medial meniscus.[12,46] Variation in the water content was observed to be consistent in the NIR region.[33] This is due to the full-depth tissue penetration of light in this region. The reverse is the case in the VIS region of the spectrum, which is restricted to the superficial layer of the meniscus.

The effect of preprocessing on the performance of models developed using spectral data from the NIR optical region is shown in Table 1. Models based on data from the NIR region (750 to 1100 nm) gave high correlation ($83.0\% \leq R^2 \leq 90.8\%$) with the biomechanical properties of human meniscus [Table 1, Figs. 5(a), 5(c)–6(a), and 6(c)] with low error. Models developed using spectral data from the VIS region (400 to 750 nm) were observed to be inferior to that based on the NIR region. Using six to eight principal components was optimal for modeling the relationship between the NIR spectral data and biomechanical properties of the meniscus samples.

From the generalized mixed model analyses, statistically significant differences in the biomechanical properties of samples obtained from the different anatomical locations of the menisci were observed in all parameters: E_{eq} ($p = 0.038$), E_{dyn} ($p < 0.001$), E_{ε} ($p < 0.001$), and M_k ($p = 0.044$). The Bland–Altman plots [Figs. 5(b), 5(d)–6(b), and 6(d)] show agreement between the predicted and measured biomechanical parameters of the samples. The bias between the predicted and measured values was negligibly small (0.01%) for all

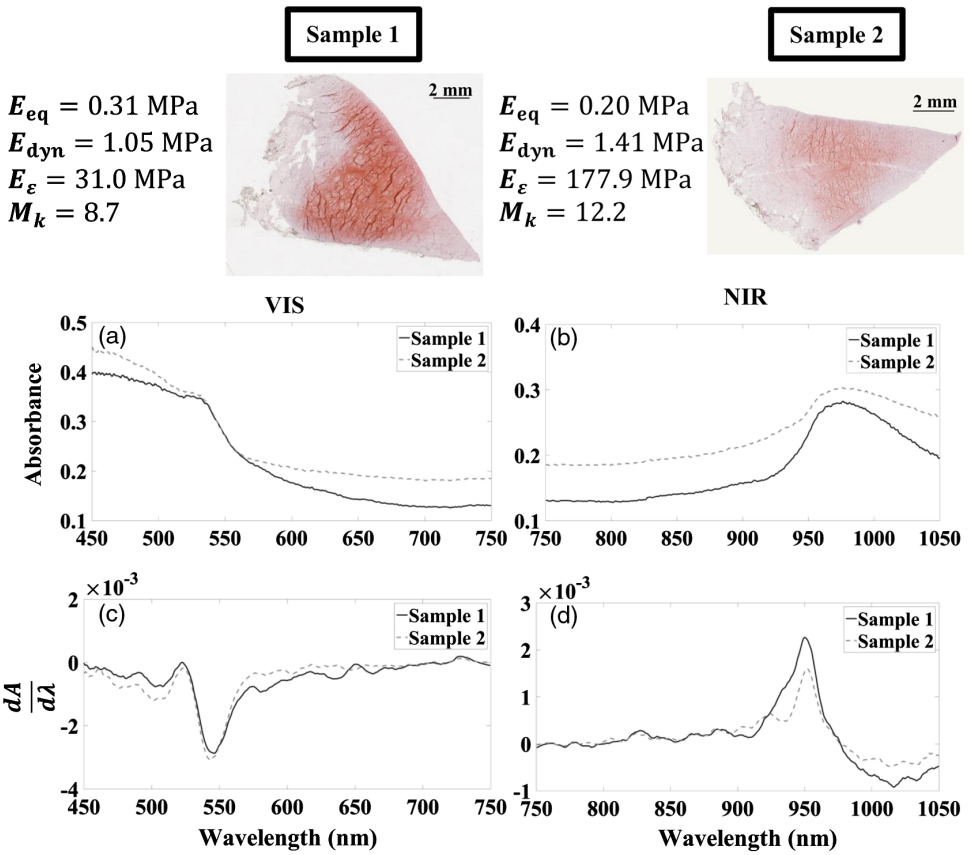

Fig. 4 Safranin-O stained human menisci sections and their corresponding raw (a–b) and first derivative preprocessed spectra (c–d). Sample 1 was extracted from the posterior part of a lateral meniscus and sample 2 from the anterior part of a medial meniscus.

Table 1 The effect of different spectral preprocessing methods on PLS model performance for predicting biomechanical properties of meniscus. (Raw: no preprocessing; SG2D, Savitzky–Golay second derivative; SNV, standard normal variate; MSC, multiplicative scatter correction; n_{comp}, number of components used in the model).

	E_{eq}				E_{dyn}			
A	R^2 (%)	RMSECV (%)	RMSEP (%)	n_{comp}	R^2 (%)	RMSECV (%)	RMSEP (%)	n_{comp}
Raw	**88.1**	**9.0**	**7.1**	**8**	87.1	8.3	8.6	7
SG2D	76.2	10.4	9.4	7	82.2	9.4	8.2	7
SNV	80.2	9.2	10.1	6	**83.1**	**8.0**	**9.6**	**6**
MSC	83.1	9.5	9.7	6	81.4	8.7	8.9	6
	E_{ε}				M_k			
B	R^2 (%)	RMSECV (%)	RMSEP (%)	n_{comp}	R^2 (%)	RMSECV (%)	RMSEP (%)	n_{comp}
Raw	79.7	7.4	9.5	7	90.5	10.7	9.4	8
SG2D	75.4	8.3	9.5	6	76.9	11.8	12.4	7
SNV	75.5	7.2	8.5	6	**90.8**	**10.8**	**8.9**	**8**
MSC	**83.0**	**7.8**	**8.4**	**6**	81.6	10.7	12.3	6

Note: The bold values represent the best preprocessing method found in the study for specific biomechanical variable.

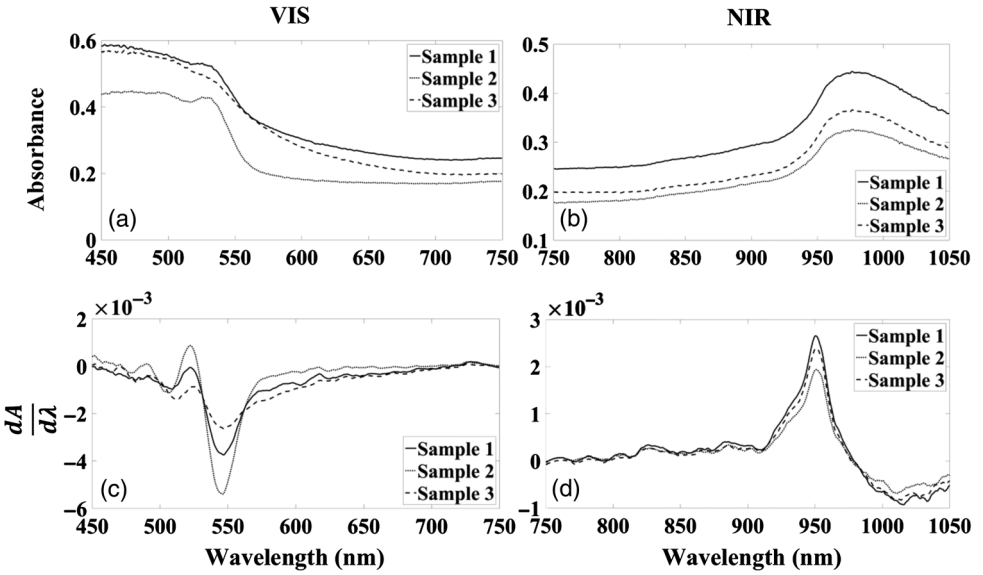

Fig. 5 Comparison of corresponding raw spectra (a–b) and first derivative preprocessed spectra (c–d) from different human menisci samples extracted from the central part of a lateral meniscus (sample 1: $E_{eq} = 0.29$ MPa, sample 2: $E_{eq} = 0.08$ MPa, and sample 3: $E_{eq} = 0.15$ MPa).

the parameters. The range and mean ± 95% confidence interval of the reference values used in model creation are E_{eq} (0.03 to 0.61 MPa and 0.2 ± 0.023 MPa), E_{dyn} (0.08 to 3.42 MPa and 0.8 ± 0.13 MPa), E_ε (0.55 to 177.93 MPa and 28.3 ± 6.64 MPa), and M_k (0.19 to 44.56 MPa, 12.6 ± 2.38 MPa).

4 Discussion

In this study, we investigated for the first time the relationship between the biomechanical properties of the human meniscus and its optical response. We demonstrated the capability of optical spectroscopy in the NIR spectral range to estimate the biomechanical properties of the human meniscus. When compared with a high-frequency intra-articular ultrasound technique (E_{eq} $R^2 = 0.49$, RMSECV = 0.08),[50] our results suggest that NIR spectroscopy (E_{eq} $R^2 = 0.88$, RMSECV = 0.05) is a more viable candidate for nondestructive assessment of meniscus biomechanical properties, outperforming the acoustic technique in terms of accuracy and error.

The outcome of the present study is consistent with the existing literature on the relationship between the spectral response and the functional properties of articular cartilage,[19,20,22,29] which resembles meniscus in terms of composition.[11,12] Although the structure of meniscus differs from that of articular cartilage, it has similar fibrous (collagen-based) protein content. Having established the relationship between meniscus biomechanical integrity and its collagen orientation/structure,[51] we recently demonstrated the potential of NIR spectroscopy for estimating human meniscus ECM composition, including collagen and PG contents determined biochemically.[33] This is due to the sensitivity of NIR spectroscopy to the physical, chemical, and morphological properties of soft tissues.[22,24,28,30,31,52]

NIR spectroscopy is sensitive to micro- and macroscopic changes in soft tissue structure and composition.[20,22] Equilibrium and dynamic moduli have been shown to be influenced by the PG and water contents.[53] The modeled strain-dependent parameters, E_ε and M_k, which are related to the structural integrity of meniscus, are influenced by the PG and collagen contents and collagen orientation, and the effects are site-specific.[51] Thus, predicting these parameters could provide information on the functional integrity of meniscus as an indirect indicator of tissue health. While there are inherent variations in meniscus composition depending on location,[12,46] an earlier study has shown that the composition also changes with injury and other pathological conditions.[11] In addition, Herwig et al.[11] reported significant variation in meniscus water, collagen, and PG contents between different stages of degeneration, and demonstrated that this variation was not age-dependent. Thus, the spectral differences observed in this study were associated with site-specific variations in meniscus composition, biomechanics, and overall condition, although the donor cadavers did not have a history of joint diseases. Nevertheless, significant spectral changes are expected as degeneration, which alters meniscus composition, progresses.[11]

Light in the NIR region penetrates deep into the tissue and allows full-thickness probing of meniscus properties. Since spectral absorption of biological materials in the NIR range arises predominantly from C─H, N─H, O─H, and S─H bonds,[54,55] which constitutes the fundamental structure of meniscus matrix components, data in this region are indicative of changes in meniscus composition, which is directly related to its function (composition–function relationship). This depth-penetrating capacity of light in the NIR region resulted in high correlation (Figs. 6 and 7, Table 1) between the measured and predicted biomechanical properties ($83.0\% \leq R^2 \leq 90.8\%$). Although meniscus possesses similar matrix composition as articular cartilage, the exact behavior (reflection/scattering) and penetration of light in the tissue is unknown and is likely to differ from that of cartilage, due to the differences in orientation of the collagen fibers and in the PG content. Understanding of this interaction would require further investigation, possibly through modeling of light propagation and depth-resolved spectroscopy. Scatter correction preprocessing methods were optimal for prediction of E_{dyn}, E_ε, and M_k. These methods attempt to minimize variations between the

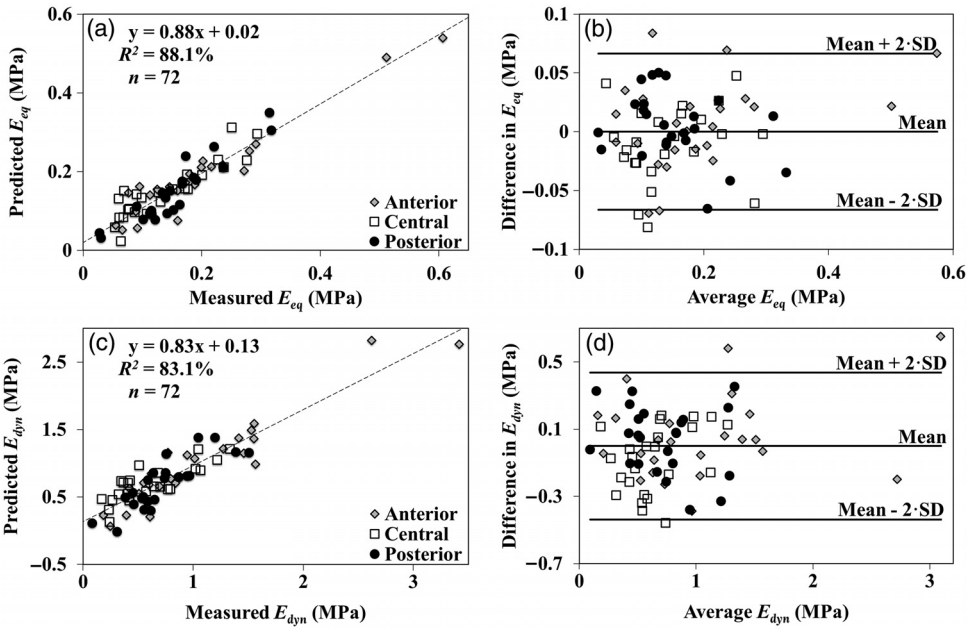

Fig. 6 Relationship between the values of NIR predicted and measured moduli [E_{eq} and E_{dyn} in (a) and (c), respectively] for the human meniscus samples; $p < 0.0001$. Bland–Altman plot illustrates agreement of the values of predicted and measured moduli (b and d). There are 24 samples in each group (anterior, central, and posterior) (E_{eq}, equilibrium modulus; E_{dyn}, dynamic modulus).

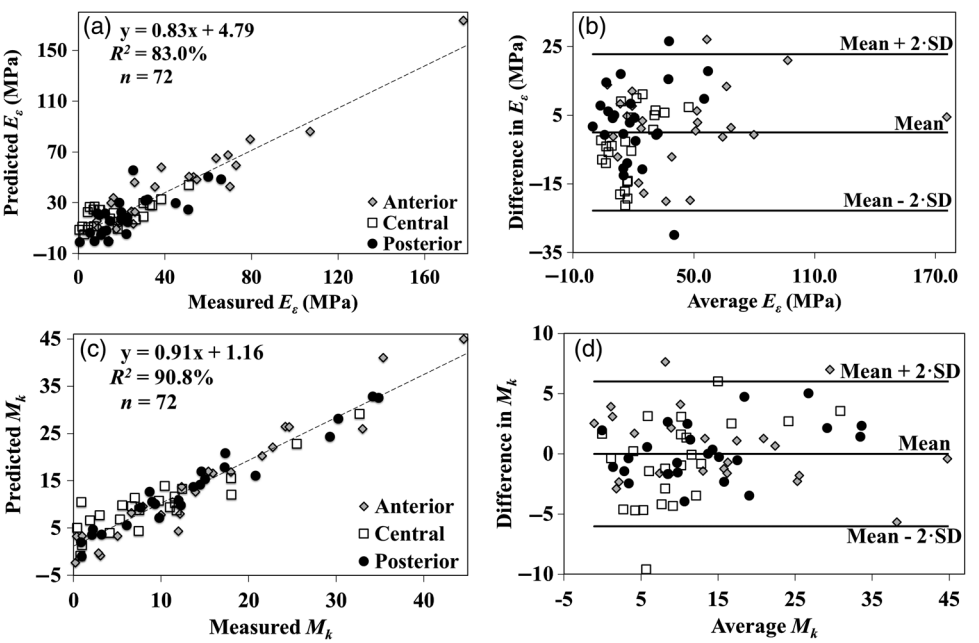

Fig. 7 Relationship between the values of NIR predicted and measured moduli [E_ε and M_k in (a) and (c), respectively] for the human meniscus samples; $p < 0.0001$. Bland–Altman plot illustrates agreement of the values of predicted and measured moduli (b and d). There are 24 samples in each group (anterior, central, and posterior) (E_ε, strain-dependent fibril network modulus; M_k, permeability strain-dependency coefficient).

samples due to light scatter by centering the spectra relative to the mean spectrum. The errors observed in the developed models are expected to decrease as sample size and variance between the samples increase.

Some samples (from the anterior horn of the meniscus) appear to be outliers; however, they were not excluded from the study. Standard practice requires that more information, such as accuracy of spectral data acquisition and inspection of the suspected samples, be checked before excluding the samples from further analysis.[56,57] The samples fulfilled these requirements and thus were retained. In addition, it is advantageous to retain such samples so that new samples with similar characteristics can be correctly predicted by the model.

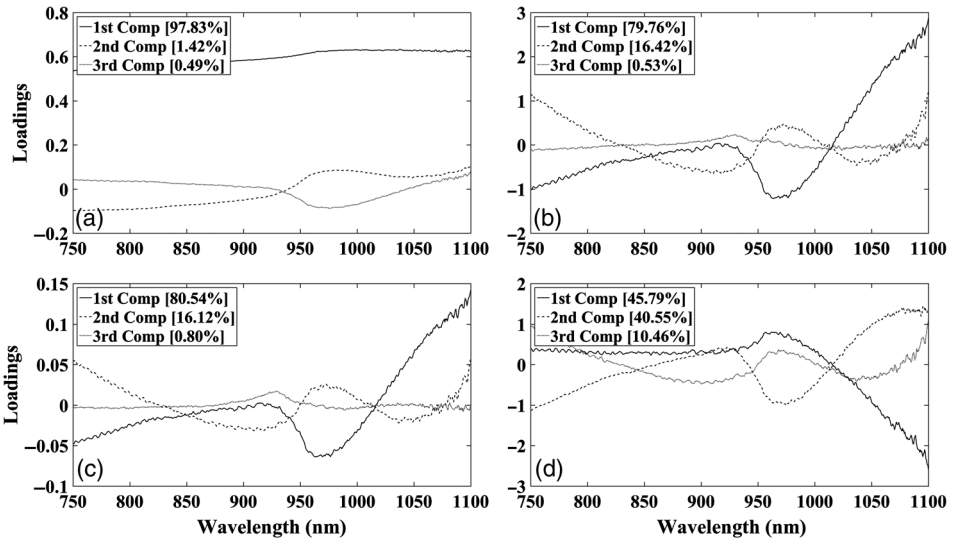

Fig. 8 PLS loading plots of the first three components of (a) E_{eq}, (b) E_{dyn}, (c) E_{ε}, and (d) M_k with the corresponding variances explained by each component (E_{eq}, equilibrium modulus; E_{dyn}, dynamic modulus; E_{ε}, strain-dependent fibril network modulus; M_k, permeability strain-dependency coefficient).

The first three PLS loadings based on the NIR spectral region, which account for the highest variance in the spectral data and indicate the contribution of specific spectral regions to the PLS model used in predicting the different biomechanical properties, are shown in Fig. 8. The loading weights associated with the NIR spectra of meniscus, like articular cartilage,[31,29] incorporate unique spectral features characteristic of the fluid (water) and solid (collagen and PGs) constituents of the matrix. Water-related absorption, evident by the dominant water peak between 950 and 977 nm [Figs. 4(b) and 4(d)], indicates strong contribution of meniscus water content to the correlation between its spectral data and biomechanical parameters. Noticeable contributions from the C—H peak between 830 and 845 nm, attributable to the solid matrix components of meniscus,[58] can be observed as well. The loading plots suggest that meniscus water content contributes significantly via the second principal component to the predictive models of E_{eq}, E_{dyn}, and E_{ε}, and via the first and third principal components in the case of M_k.

A possible limitation of the current study is that the effect of blood in the tissue's spectral response was not accounted for, as the blood in the samples was flushed out prior to storage and measurement. Blood is a major absorber of light and its effect on the spectrum requires further investigation. Thus, further optimization of the method and protocol is required before the method can be applied for *in vivo* use. In addition, further studies are required to investigate the variation in biomechanical properties between the different meniscus zones (i.e., red–red, red–white, and white–white). Since meniscus properties are site-specific, a potential extension of the optical technique would be to map the spatial distribution of meniscus biomechanical properties. We have previously demonstrated this concept for articular cartilage[59,60] using NIR spectroscopy. However, spatial mapping of meniscus properties was not conducted in this study as there were too few measurement locations per meniscus, and mapping was not part of the aim of the present study.

The number of samples used to develop the models in this study was limited. Large number of samples from patients with varying meniscus condition would be needed to develop a more robust model prior to *in vivo* application. In future studies, different types of meniscal injuries and degeneration would need to be considered with respect to how they affect the optical properties of the tissue and how different the variation between healthy and damaged meniscus is from the site-specific variation.

It is worth noting that the samples were obtained from cadavers with no history of joint diseases, thus they do not necessarily represent the full range of meniscus conditions (including normal and different levels of degeneration) expected in human patients. Additionally, the experimental setup adopted in this study is not optimal for clinical application; nevertheless, this does not alter the underlying hypothesis and outcome of the study. The measurement setup can easily be modified for arthroscopic application, e.g., by integrating the spectrometer light source and detector into one unit applied via a contact optical fiber probe.

5 Conclusion

Optical absorption spectrum of human meniscus, in the NIR spectral range, correlates with its biomechanical properties. NIR spectroscopy is a potential method for rapid and nondestructive evaluation of human meniscus mechanical integrity and health in real-time during arthroscopic surgery. For holistic characterization of overall meniscus health and deterioration *in vivo*, we propose a combination of both predicted biochemical composition[33] and biomechanical integrity. However, further study is required to optimize the method for *in vivo* application.

Disclosures

The authors have no conflicts of interest or financial interests in the execution of this study and preparation of the article.

Acknowledgments

This study was supported by funding from the Academy of Finland (project 267551, University of Eastern Finland) and Kuopio University Hospital (VTR projects 5041750 and 5041744, PY210 Clinical Neurophysiology). Dr. Afara would like to acknowledge the Finnish Cultural Foundation (00160079).

References

1. O. C. Brantigan and A. F. Voshell, "The mechanics of the ligaments and menisci of the knee joint," *J. Bone Jt. Surg. Am.* **23**(1), 44–66 (1941).
2. K. L. Markolf, J. S. Mensch, and H. C. Amstutz, "Stiffness and laxity of the knee—the contributions of the supporting structures. A quantitative in vitro study," *J. Bone Jt. Surg. Am.* **58**(5), 583–594 (1976).
3. P. S. Walker and M. J. Erkman, "The role of the menisci in force transmission across the knee," *Clin. Orthop. Relat. Res.* **109**, 184–192 (1975).
4. M. D. Bird and M. B. Sweet, "A system of canals in semilunar menisci," *Ann. Rheum. Dis.* **46**(9), 670–673 (1987).
5. J. C. Kennedy, I. J. Alexander, and K. C. Hayes, "Nerve supply of the human knee and its functional importance," *Am. J. Sports Med.* **10**(6), 329–335 (1982).
6. C. A. McDevitt and R. J. Webber, "The ultrastructure and biochemistry of meniscal cartilage," *Clin. Orthop. Relat. Res.* **252**, 8–18 (1990).
7. H. S. Cheung, "Distribution of type I, II, III and V in the pepsin solubilized collagens in bovine menisci," *Connect. Tissue Res.* **16**(4), 343–356 (1987).
8. W. Petersen and B. Tillmann, "Collagenous fibril texture of the human knee joint menisci," *Anat. Embryol.* **197**(4), 317–324 (1998).
9. S. P. Arnoczky and R. F. Warren, "Microvasculature of the human meniscus," *Am. J. Sports Med.* **10**(2), 90–95 (1982).
10. A. J. S. Fox et al., "The human meniscus: a review of anatomy, function, injury, and advances in treatment," *Clin. Anat.* **28**(2), 269–287 (2015).
11. J. Herwig, E. Egner, and E. Buddecke, "Chemical changes of human knee joint menisci in various stages of degeneration," *Ann. Rheum. Dis.* **43**(4), 635–640 (1984).
12. D. C. Fithian, M. A. Kelly, and V. C. Mow, "Material properties and structure-function relationships in the menisci," *Clin. Orthop. Relat. Res.* **252**, 19–31 (1990).
13. W. B. Wheatley, J. Krome, and D. F. Martin, "Rehabilitation programmes following arthroscopic meniscectomy in athletes," *Sports Med.* **21**(6), 447–456 (1996).
14. K. M. Fischenich et al., "Effects of degeneration on the compressive and tensile properties of human meniscus," *J. Biomech.* **48**(8), 1407–1411 (2015).
15. E. K. Danso et al., "Characterization of site-specific biomechanical properties of human meniscus—importance of collagen and fluid on mechanical nonlinearities," *J. Biomech.* **48**(8), 1499–1507 (2015).
16. X. Ayral et al., "Inter-observer reliability of the arthroscopic quantification of chondropathy of the knee," *Osteoarthritis Cartilage* **6**(3), 160–166 (1998).
17. B. H. Brismar et al., "Observer reliability in the arthroscopic classification of osteoarthritis of the knee," *J. Bone Joint Surg. Br.* **84**(1), 42–47 (2002).
18. G. Spahn et al., "Near-infrared spectroscopy for arthroscopic evaluation of cartilage lesions: results of a blinded, prospective, interobserver study," *Am. J. Sports Med.* **38**(12), 2516–2521 (2010).
19. I. O. Afara, S. Singh, and A. Oloyede, "Load-unloading response of intact and artificially degraded articular cartilage correlated with near infrared (NIR) absorption spectra," *J. Mech. Behav. Biomed. Mater.* **20**, 249–258 (2013).
20. G. Spahn et al., "Evaluation of cartilage defects with near-infrared spectroscopy (NIR): an ex vivo study," *Med. Eng. Phys.* **30**(3), 285–292 (2008).
21. A. Hanifi et al., "Fourier transform infrared imaging and infrared fiber optic probe spectroscopy identify collagen type in connective tissues," *PLoS One* **8**(5), e64822 (2013).
22. J. K. Marticke et al., "How do visual, spectroscopic and biomechanical changes of cartilage correlate in osteoarthritic knee joints?" *Clin. Biomech.* **25**(4), 332–340 (2010).
23. M. V. Padalkar and N. Pleshko, "Wavelength-dependent penetration depth of near infrared radiation into cartilage," *Analyst* **140**(7), 2093–2100 (2015).
24. I. Afara, S. Singh, and A. Oloyede, "Application of near infrared (NIR) spectroscopy for determining the thickness of articular cartilage," *Med. Eng. Phys.* **35**(1), 88–95 (2013).
25. A. Hanifi et al., "Infrared fiber optic probe evaluation of degenerative cartilage correlates to histological grading," *Am. J. Sports Med.* **40**(12), 2853–2861 (2012).
26. P. H. Puhakka et al., "Estimation of articular cartilage properties using multivariate analysis of optical coherence tomography signal," *Osteoarthritis Cartilage* **23**(12), 2206–2213 (2015).
27. D. A. Burns and E. W. Ciurczak, *Handbook of Near-Infrared Analysis*, 3rd ed., p. 393, CRC Press, Boca Raton, Florida (2007).
28. I. O. Afara et al., "Near infrared spectroscopy for rapid determination of Mankin score components: a potential tool for quantitative characterization of articular cartilage at surgery," *Arthroscopy* **30**(9), 1146–1155 (2014).
29. I. O. Afara et al., "Optical absorption spectra of human articular cartilage correlate with biomechanical properties, histological score and biochemical composition," *Physiol. Meas.* **36**(9), 1913–1928 (2015).
30. M. V. Padalkar, R. G. Spencer, and N. Pleshko, "Near infrared spectroscopic evaluation of water in hyaline cartilage," *Ann. Biomed. Eng.* **41**(11), 2426–2436 (2013).
31. U. P. Palukuru, C. M. McGoverin, and N. Pleshko, "Assessment of hyaline cartilage matrix composition using near infrared spectroscopy," *Matrix Biol.* **38**, 3–11 (2014).
32. E. J. Kucharz, "Structure, heterogeneity, and distribution," in *The Collagens: Biochemistry and Pathophysiology*, E. J. Kucharz, Ed., pp. 5–29, Springer, Berlin, Heidelberg (1992).
33. J. Ala-Myllymäki et al., "Optical spectroscopic determination of human meniscus composition," *J. Orthop. Res.* **34**(2), 270–278 (2016).
34. A. Johansson et al., "A spectroscopic approach to imaging and quantification of cartilage lesions in human knee joints," *Phys. Med. Biol.* **56**(6), 1865–1878 (2011).
35. P. E. Gelber et al., "Freezing causes changes in the meniscus collagen net: a new ultrastructural meniscus disarray scale," *Knee Surg. Sports Traumatol. Arthrosc.* **16**(4), 353–359 (2008).
36. P. E. Gelber et al., "Cryopreservation does not alter the ultrastructure of the meniscus," *Knee Surg. Sports Traumatol. Arthrosc.* **17**(6), 639–644 (2009).
37. S. Ahmad, V. A. Singh, and S. I. Hussein, "Cryopreservation versus fresh frozen meniscal allograft: a biomechanical comparative analysis," *J. Orthop. Surg.* **25**(3), 230949901772794 (2017).
38. R. K. Korhonen et al., "Comparison of the equilibrium response of articular cartilage in unconfined compression, confined compression and indentation," *J. Biomech.* **35**(7), 903–909 (2002).
39. I. Kutzner et al., "Loading of the knee joint during activities of daily living measured in vivo in five subjects," *J. Biomech.* **43**(11), 2164–2173 (2010).
40. F. Liu et al., "In vivo tibiofemoral cartilage deformation during the stance phase of gait," *J. Biomech.* **43**(4), 658–665 (2010).
41. W. C. Hayes et al., "A mathematical analysis for indentation tests of articular cartilage," *J. Biomech.* **5**(5), 541–551 (1972).
42. G. A. Ateshian, B. J. Ellis, and J. A. Weiss, "Equivalence between short-time biphasic and incompressible elastic material responses," *J. Biomech. Eng.* **129**(3), 405–412 (2007).
43. P. Julkunen et al., "Characterization of articular cartilage by combining microscopic analysis with a fibril-reinforced finite-element model," *J. Biomech.* **40**(8), 1862–1870 (2007).
44. R. K. Korhonen et al., "Fibril reinforced poroelastic model predicts specifically mechanical behavior of normal, proteoglycan depleted and collagen degraded articular cartilage," *J. Biomech.* **36**(9), 1373–1379 (2003).
45. L. P. Li, M. D. Buschmann, and A. Shirazi-Adl, "A fibril reinforced nonhomogeneous poroelastic model for articular cartilage: inhomogeneous response in unconfined compression," *J. Biomech.* **33**(12), 1533–1541 (2000).
46. J. T. J. Honkanen et al., "Contrast enhanced imaging of human meniscus using cone beam CT," *Osteoarthritis Cartilage* **23**(8), 1367–1376 (2015).
47. W. Wilson et al., "Stresses in the local collagen network of articular cartilage: a poroviscoelastic fibril-reinforced finite element study," *J. Biomech.* **37**(3), 357–366 (2004).
48. A. van der Voet, "A comparison of finite element codes for the solution of biphasic poroelastic problems," *Proc. Inst. Mech. Eng. H.* **211**(2), 209–211 (1997).
49. R. L. Spilker, J. K. Suh, and V. C. Mow, "A finite element analysis of the indentation stress-relaxation response of linear biphasic articular cartilage," *J. Biomech. Eng.* **114**(2), 191–201 (1992).

50. T. Viren et al., "Ultrasound assessment of human meniscus," *Ultrasound Med. Biol.* **43**(9), 1753–1763 (2016).
51. E. K. Danso et al., "Structure-function relationships of human meniscus," *J. Mech. Behav. Biomed. Mater.* **67**, 51–60 (2017).
52. I. Afara et al., "Non-destructive evaluation of articular cartilage defects using near-infrared (NIR) spectroscopy in osteoarthritic rat models and its direct relation to Mankin score," *Osteoarthrosis Cartilage* **20**(11), 1367–1373 (2012).
53. P. Bursac, S. Arnoczky, and A. York, "Dynamic compressive behavior of human meniscus correlates with its extra-cellular matrix composition," *Biorheology* **46**(3), 227–237 (2009).
54. I. O. Afara, Z. Pawlak, and A. Oloyede, "Current state of the application of infrared optical methods for assessing articular cartilage," *J. Mater. Sci. Eng. A* **1**(6), 1–7 (2011).
55. I. Afara, T. Sahama, and A. Oloyede, "Near infrared for non-destructive testing of articular cartilage," in *Nondestructive Testing of Materials and Structures*, RILEM Bookseries, Vol. **6**, pp. 399–404, Springer, Dordrecht (2013).
56. C. E. Miller, "Chemometrics for on-line spectroscopy applications—theory and practice," *J. Chemom.* **14**(5–6), 513–528 (2000).
57. C. E. Miller, "Chemometrics in process analytical chemistry," in *Process Analytical Technology*, K. A. Bakeev, Ed., pp. 226–328, Blackwell Publishing Ltd., Oxford (2005).
58. B. H. Stuart, "Organic Molecules," in *Infrared Spectroscopy: Fundamentals and Applications*, D. J. Ando, Ed., p. 86, John Wiley & Sons, Inc., New York (2005).
59. J. K. Sarin et al., "Near infrared spectroscopic mapping of functional properties of equine articular cartilage," *Ann. Biomed. Eng.* **44**(11), 3335–3345 (2016).
60. I. O. Afara et al., "Spatial mapping of proteoglycan content in articular cartilage using near-infrared (NIR) spectroscopy," *Biomed. Opt. Express* **6**(1), 144–154 (2015).

Juho Ala-Myllymäki received his BSc degree in physics from the University of Jyväskylä and his MSc degree in applied physics from the University of Eastern Finland in 2014 and 2017, respectively. He is a research assistant at the Biophysics of Bone and Cartilage Group, Department of Applied Physics, University of Eastern Finland. His current research interest includes adaptation of near-infrared spectroscopy for diagnosis of meniscus pathologies.

Elvis K. Danso started his postdoctoral research fellowship at Colorado State University (Mechanical Engineering Department, Soft Tissue Mechanics Laboratory) in March 2017. Prior to that, he obtained both his master's (medical physics) and PhD (applied physics) degrees from the University of Eastern Finland. In Finland, he worked in the Biophysics of Bone and Cartilage Research Group. His current research interests include biomechanical characterization of orthopaedic soft tissues and strategies to halt the progression of osteoarthritis.

Juuso T. J. Honkanen received his MSc and PhD degrees in medical physics from the University of Eastern Finland in 2012 and 2016, respectively. Currently, he works at the Cancer Center of the Kuopio University Hospital, Finland, as an assistant medical physicist. His research interests include contrast-enhanced computed tomography of articular cartilage and meniscus.

Rami K. Korhonen received his MSc and PhD degrees in the Department of Physics, University of Kuopio, Finland, in 2000 and 2004, respectively. From 2005 to 2007, he was a postdoctoral fellow in Human Performance Laboratory, University of Calgary, Canada. Currently, he is a professor of biomechanics at the Department of Applied Physics, University of Eastern Finland. His current research interests include soft tissue and cell biomechanics, multiscale imaging and modeling, and development of knee joint models for diagnostics and prediction of osteoarthritis.

Juha Töyräs received his MSc and PhD degrees in medical physics from the University of Kuopio in 1999 and 2001, respectively. He is a professor of medical physics and engineering at the Department of Applied Physics, University of Eastern Finland. He also serves as a chief physicist with the Diagnostic Imaging Centre, Kuopio University Hospital. His current research interests include development of quantitative ultrasound, arthroscopy, and computed tomography methods for diagnostics of osteoporosis and osteoarthrosis.

Isaac O. Afara received his BS degree (Hons., electrical/electronics engineering) from the University of Lagos, Nigeria, in 2006 and his PhD (medical engineering) from Queensland University of Technology, Australia, in 2012. He was a postdoctoral fellow in the Biophysics of Bone and Cartilage Group, Department of Applied Physics, University of Eastern Finland in 2014–2015, where he is currently adjunct professor of Biomedical Spectroscopy. His research is focused on adaptation of optical techniques for diagnosis of soft tissue pathologies.